POLYPUBLIE

Scalable probabilistic deterioration model based on visual inspections and structural attributes from large networks of bridges

Said Ali Kamal Fakhri, Zachary Hamida, James Alexandre Goulet

Document en libre accès dans PolyPublie
Open Access document in PolyPublie

Date	2025
Type	Article de revue / Article
Version	Version officielle de l'éditeur / Published version
URL de PolyPublie PolyPublie URL	https://publications.polymtl.ca/61948/
Évaluation par les pairs Peer reviewed	Révisé par les pairs / Refereed
Conditions d'utilisation Terms of use	Creative Commons Attribution-Utilisation non commerciale 4.0 International / Creative Commons Attribution-NonCommercial 4.0 International (CC BY-NC)
Référence Citation	Fakhri, S. A. K., Hamida, Z., & Goulet, J. A. (2025). Scalable probabilistic deterioration model based on visual inspections and structural attributes from large networks of bridges. Advanced Engineering Informatics, 64, 103035 (10 pages). https://doi.org/10.1016/j.aei.2024.103035

Publication officielle
Official publication

Titre de la revue Journal title	Advanced Engineering Informatics (vol. 64)
Maison d'édition Publisher	Elsevier
URL officielle Official URL	https://doi.org/10.1016/j.aei.2024.103035
Mention légale Legal notice	©2024 The Authors. Published by Elsevier Ltd. This is an open access article under the CC BY-NC license (http://creativecommons.org/licenses/bync/ 4.0/).

Ce fichier a été téléchargé à partir de PolyPublie, le dépôt institutionnel de Polytechnique Montréal
This file has been downloaded from PolyPublie, the institutional repository of Polytechnique Montréal
https://publications.polymtl.ca

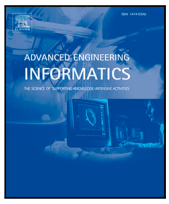
Advanced Engineering Informatics 64 (2025) 103035



Contents lists available at ScienceDirect

Advanced Engineering Informatics

journal homepage: www.elsevier.com/locate/aei



Full length article



Scalable probabilistic deterioration model based on visual inspections and structural attributes from large networks of bridges

Said Ali Kamal Fakhri, Zachary Hamida *, James-A. Goulet

Department of Civil, Geologic and Mining Engineering, Polytechnique Montreal, 2500 Chem. de Polytechnique, Montreal, H3T 1J4, QC, Canada

ARTICLE INFO

Keywords:
Visual inspections
Structural attributes
State-space models
Bayesian neural network
Inspectors uncertainty
Structural deterioration

ABSTRACT

Visual inspections of large networks of bridges yield millions of data points scattered across thousands of structural elements. Alongside visual inspections, structural attributes such as age, location and traffic load provide contextual information about the deterioration patterns in the network. Leveraging this network-scale data for modeling deterioration is challenging, especially when each structural element has few inspections over a long period of time. Moreover, as new bridge information and inspections are added each year, it is strictly important for deterioration models to be scalable. This paper addresses these challenges by proposing a scalable probabilistic approach for modeling deterioration of large networks of bridges. The new framework consists of state-space models (SSM) for modeling the deterioration based on visual inspections and a Bayesian neural network (BNN) that factors-in information about structural attributes. The role of the BNN model is to learn the mapping between the initial distribution of the deterioration speed and the structural attributes of each bridge. The new framework is shown to be computationally efficient and can seamlessly incorporate a large number of structural attributes, which alleviates the need for feature selection. In addition, the proposed framework incorporates a new approach for learning the inspectors' uncertainty parameters which is shown to provide better generalization. The experiments in this study are based on real data from the network of bridges in the province of Quebec, Canada.

1. Introduction

Deterioration of transportation infrastructure due to aging, usage, and environmental exposure is an issue faced by most industrialized countries [1]. Addressing this issue can be done by making timely maintenance decisions, which primarily rely on information from structural health monitoring systems [2]. The predominant approach to monitoring the health of bridges is based on periodic visual inspections that assess their structural health at the structural element level [3–5]. Even though inspections of bridge networks produce millions of inspection data points, they are spread over thousands of structural components. Effectively, this implies that many structural elements have few inspections over long periods of time.

The scarcity of inspection data at the "structural element" level is further compounded by the subjective nature of inspections, which results in highly variable observations [3,6–8]. For instance, two inspectors may assign different condition ratings to the same structural element depending on their level of experience [9]. Despite these challenges, visual inspection-based deterioration models remain to be an essential component in decision-making and maintenance planning [10,11].

Notable examples include discrete Markov models (DMMs) [12–15] which primarily focus on learning the transition probabilities across the deterioration states. DMMs have found a large adoption in practice due to their simplicity; however, existing limitations in DMMs can restrict their overall effectiveness. DMMs assume all inspectors to have the same observation error [6], and their capacity to provide a probabilistic estimates for the deterioration speed and effect of interventions are limited [6,16]. Hierarchical Bayesian models were also applied for modeling deterioration [17]; however, their application was limited in scale due to relying on computationally expensive sampling methods such as Markov chain Monte Carlo (MCMC) to approximate the posterior probability distribution. Existing work that aimed at alleviating the computational cost of hierarchical models attempted to replace MCMC by a computationally efficient solutions such as variational inference (VI) [17]. Nonetheless, the VI approach requires adjustments whenever a new variable is introduced (e.g., adding environmental factors) [17].

Other approaches in the literature ventured to reduce the reliance on visual inspections by incorporating contextual information such

* Corresponding author.
E-mail address: zachary.hamida@gmail.com (Z. Hamida).

https://doi.org/10.1016/j.aei.2024.103035
Received 26 May 2024; Received in revised form 28 October 2024; Accepted 4 December 2024
Available online 15 December 2024
1474-0346/© 2024 The Authors. Published by Elsevier Ltd. This is an open access article under the CC BY-NC license (http://creativecommons.org/licenses/by-nc/4.0/).

as material, age and location alongside visual inspection data. Existing studies demonstrated applications using feed-forward neural networks [18–21]. An example application includes the development of a multi-layer perceptron (MLP) classifier model to predict the next condition state of a bridge deck by using features such as, the previous condition, age and maintenance history [18]. Despite their capacity to scale, regression-based models remain limited in effectively capturing deterioration patterns from visual inspection data. A primary challenge is the highly imbalanced nature of inspection datasets, as most bridges are maintained in good condition and seldom reach severe deterioration states. Furthermore, the sparse inspection data at the "structural element" level limit the capacity of these models to track the time-dependent progression of deterioration accurately. In addition to contextual information, physical models such as analytical carbonation-induced corrosion model [22], and an empirical chloride-induced corrosion model [23] have been also considered; however, they require extensive knowledge about each structure (e.g., information from original design documents, various tests and measurements, etc.), thus limiting their scalability.

Challenges in scalability and uncertainty quantification have prompted the adoption of state-space models (SSMs) as a deterioration model [6]. SSM model stands out as it provides modeling advantages such as, quantifying the uncertainty associated with each inspector and the probabilistic estimation of the deterioration speed [9]. Existing variations of the SSM model includes a model that relies only on visual inspection data [6], and a model that factors structural attributes along with visual inspections [24]. In the latter model, factoring structural attributes was done by coupling the SSM framework with kernel regression (KR) [24]. While this hybrid model maintains the advantages attained from using the SSM framework, it suffers from computational inefficiency and limited capacity in incorporating structural attributes, as it only allows for up to six structural attributes and takes significant computing resources and time to train [24]. In addition, the application of the SSM-KR model was demonstrated on visual inspection data where the uncertainty associated with each inspector is represented by un-biased observation errors.

This paper proposes a hybrid deterioration model that couples the SSM with a Bayesian neural network (BNN) to effectively incorporate the structural attributes in the deterioration analyses. This new hybrid model provides direct solutions to the highlighted limitations in the SSM-KR framework by, (1) being computationally efficient and significantly reduce the compute time for training, and (2) being scalable which enables considering all available information about the structural attributes. Furthermore, the parameters of the proposed deterioration model are estimated using a new estimation framework, which reduces the total number of model parameters and is shown to improve the model predictive capacity when evaluated on an independent test set. The new parameter estimation addresses the limitation of having few inspections performed by an inspector on a specific category of elements (e.g., slabs) compared to other structural categories (e.g., beams). The numerical analyses in this study includes comparing the performance of the SSM-BNN model against the existing SSM-KR model. The validation analyses are performed using data from the network of bridges in the Quebec province, Canada.

2. Problem context

A network consists of a set of bridges $\{\mathcal{B}_1, \mathcal{B}_2, \ldots, \mathcal{B}_{\mathrm{B}}\}$ with each bridge $\mathcal{B}_j$ encompassing multiple structural elements e_p^j. Each structural elements can be characterized by its health state and its structural attributes. The health state in this context is evaluated over time using visual inspections, while the structural attributes encompass attributes directly related to the element (e.g., material) and attributes that are related to the bridge (e.g., bridge location). Fig. 1 provides an illustrative example about the bridge data considered in this study.

Fig. 1, shows that despite variations in the health condition among the structural elements, the deterioration speed patterns can have similar curve-shapes between structures sharing similar structural attributes. Note that the similarity hypothesis serve only as a motivation to conduct this research work, rather than being a necessary assumption; as the main objective in this study is to learn the relationship between structural attributes and the deterioration speed across multiple bridges using a data-drive approach, in order to improve the predictive capacity of deterioration models based on visual inspections.

3. Background

This section provides the theoretical background for the existing methods related to the proposed probabilistic deterioration model.

3.1. State-space models

State-space models (SSM) describe the behavior of a system over time using probabilistic transition and observation models. SSMs have been shown to be effective at modeling infrastructure deterioration on a network-scale [6], where the transition model describes the physical deterioration process following,

$$\overbrace{\boldsymbol{x}_t = \mathbf{A}\boldsymbol{x}_{t-1} + \boldsymbol{w}_t}^{\text{transition model}}, \quad \overbrace{\boldsymbol{w}_t : \boldsymbol{W} \sim \mathcal{N}(\boldsymbol{w}; \mathbf{0}, \mathbf{Q})}^{\text{process errors}}. \tag{1}$$

Here, $\boldsymbol{x}_t = [x_t \ \dot{x}_t \ \ddot{x}_t]^{\intercal}$ is the hidden state vector at time t containing the condition x_t, speed $\dot{x}_t$, and acceleration $\ddot{x}_t$ of a structural element, $\mathbf{A}$ is the state transition matrix, $\boldsymbol{w}_t$ is the process error, and $\mathbf{Q}$ is the process error covariance matrix. The state transition matrix and its associated process error covariance matrix are derived assuming a constant-acceleration kinematic model,

$$\mathbf{A} = \begin{bmatrix} 1 & \Delta t & \frac{\Delta t^2}{2} \\ 0 & 1 & \Delta t \\ 0 & 0 & 1 \end{bmatrix}, \quad \mathbf{Q} = \sigma_W^2 \begin{bmatrix} \frac{\Delta t^4}{4} & \frac{\Delta t^3}{2} & \frac{\Delta t^2}{2} \\ \frac{\Delta t^3}{2} & \Delta t^2 & \Delta t \\ \frac{\Delta t^2}{2} & \Delta t & 1 \end{bmatrix}, \tag{2}$$

where Δt is the time step between successive states and σ_W^2 is the variance of the process error [6]. The uncertainty of visual inspections are characterized by the observation model described by,

$$\overbrace{y_t = \mathbf{C}\boldsymbol{x}_t + v_t}^{\text{observation model}}, \quad \overbrace{v_t : V \sim \mathcal{N}(v; \mu_V(i), \sigma_V^2(i))}^{\text{observation errors}}, \tag{3}$$

where y_t represents the observation at time t, $\mathbf{C} = [1\ 0\ 0]$ is the observation matrix, and v_t is the observation error with $\mu_V(i)$ and $\sigma_V^2(i)$ representing the relative bias and variance of the ith inspector [9]. The deterioration state at each time step t is inferred using the Kalman filter (KF) [25] and Rauch–Tung–Striebel (RTS) smoother [26], which are detailed in Appendix B. Using the KF to model deterioration requires imposing two constraints on the state estimates to ensure the condition x_t is monotonically decreasing over time and to keep the model predictions within a predefined range of values [6]. The first constraint is enforced at each time step by restricting the deterioration rate $\dot{x}_t$ to be negative using a probability density function (PDF) truncation method [27]. The second constraint is imposed using space transformation which preserves the hidden states and observations within a predefined range of health conditions $[l, u]$. Further details about the space transformation are provided in Appendix C. Although the SSM framework can effectively model deterioration, it solely relies on the visual inspection data without incorporating information about structural attributes [6].

3.2. State-space models with kernel regression

Augmenting the SSM framework with a kernel-based regression (KR) model enables taking into account information about structural

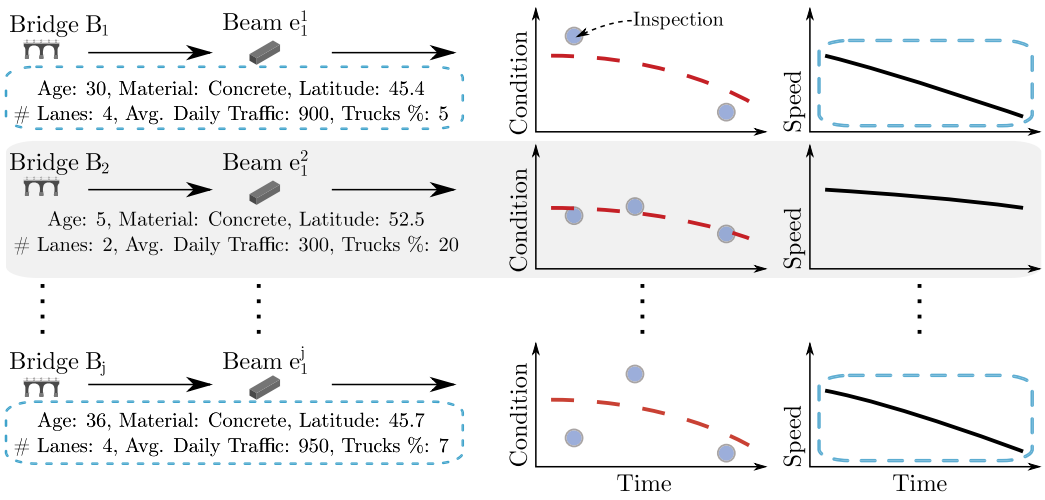


Fig. 1. Illustrative example for bridge data which shows structural attributes associated with each structural element (left) alongside the visual inspection data (right, blue points). The example demonstrates that while the deterioration condition may vary among structural elements, the patterns of deterioration speed can be similar, especially for structural elements sharing similar structural attributes. Structural elements with similarities are highlighted with a dashed-line rectangle.

attributes. The purpose of KR is to include structural attributes $\boldsymbol{z}$ in the deterioration analyses to improve the prior for each element's initial state $\boldsymbol{x}_0 = [x_0 \ \dot{x}_0 \ \ddot{x}_0]^\intercal$ by sharing information between structures. More precisely, KR predicts the deterioration speed $\dot{x}_0$ based on each element's attributes that are defined for each bridge by a vector $\boldsymbol{z}_j = [z_j^1 \ \dots \ z_j^{\mathtt{Z}}]^\intercal$. The KR method involves discretizing each of the $\mathtt{Z}$ covariates' domains with $\mathtt{M}$ reference points, which are then permuted to form a grid of $\mathtt{N} \equiv \mathtt{M}^{\mathtt{Z}}$ points denoted by $\mathbf{G} = [\boldsymbol{g}_1 \ \dots \ \boldsymbol{g}_{\mathtt{N}}]^\intercal \in \mathbb{R}^{\mathtt{N}\times\mathtt{Z}}$. Each ith grid point in $\mathbf{G}$ corresponds to a unique combination of the reference points and is associated with a deterioration rate $\dot{x}_i \in \dot{\boldsymbol{x}}_z = [\dot{x}_1 \ \dots \ \dot{x}_{\mathtt{N}}]^\intercal$. KR estimates each element's deterioration rate $\dot{x}_0$ based on the proximity of its attributes $\boldsymbol{z}_j$ to different grid points using a weighted sum given by,

$$\dot{x}_0 = \boldsymbol{a}^\intercal \dot{\boldsymbol{x}}_z + w_0, \ w_0 : W_0 \sim \mathcal{N}\left(0, \sigma_{W_0}^2\right), \tag{4}$$

where w_0 is the process error and $\boldsymbol{a} = [a_1 \ a_2 \ \dots \ a_{\mathtt{N}}]^\intercal$ is the vector of weights, which is obtained using a multivariate kernel function $\boldsymbol{k}(\cdot)$ following

$$a_i = \frac{\boldsymbol{k}\left(\boldsymbol{z}_j, \mathbf{G}_{(i)}, \boldsymbol{\ell}\right)}{\sum_{n=1}^{\mathtt{N}} \boldsymbol{k}\left(\boldsymbol{z}_j, \mathbf{G}_{(n)}, \boldsymbol{\ell}\right)}, \ i = 1, \dots, \mathtt{N}, \tag{5}$$

where $\boldsymbol{\ell} = [\ell_1 \dots \ell_{\mathtt{Z}}]^\intercal$ are the kernel bandwidths and $\mathbf{G}_{(i)}$ is the ith point on the grid. The kernel function $\boldsymbol{k} : \mathbb{R}^{\mathtt{Z}} \to \mathbb{R}$ is defined as a product of univariate kernels $k(\cdot)$ given by

$$\boldsymbol{k}\left(\boldsymbol{z}_j, \mathbf{G}_{(i)}, \boldsymbol{\ell}\right) = k\left(\frac{z_j^1 - g_i^1}{\ell_1}\right) \cdot \ldots \cdot k\left(\frac{z_j^{\mathtt{Z}} - g_i^{\mathtt{Z}}}{\ell_{\mathtt{Z}}}\right). \tag{6}$$

The parameter estimation of the SSM-KR model is detailed in the work of Hamida and Goulet [24]. Although the use of KR can improve the predictive capacity of the deterioration state, the SSM-KR model has limitations related to scalability and computationally efficiency. Specifically, the computational bottleneck is within the training of the KR model, which requires calculating the inverse of the covariance term $\dot{\boldsymbol{\Sigma}}_{0|z} \in \mathbb{R}^{\mathtt{M}^{\mathtt{Z}}\times\mathtt{M}^{\mathtt{Z}}}$, where $\mathtt{M}$ is the number of reference points for each attribute (normally $\mathtt{M} = 5$) and $\mathtt{Z}$ is the number of structural attributes [24]. Additional requirements for using KR includes the selection of its hyper-parameters, such as kernel types, which can be a lengthy process to identify. Overcoming the inherent limitations in the SSM-KR model is only possible by replacing KR with a probabilistic regression approach that is compatible with SSM, scalable and computationally efficient. Bayesian neural networks (BNN) offer such an alternative, as they provide a flexible framework for probabilistic regression that aligns well with the aforementioned requirements.

4. Methodology

This section presents a new hybrid framework for modeling infrastructure deterioration based on state-space models and a Bayesian neural network (BNN) trained via tractable approximate Gaussian inference (TAGI).

4.1. Coupling Bayesian neural networks with state-space models

In the proposed SSM-BNN model, the BNN component is used to enhance the SSM predictions by learning the relation between the attributes of structural elements (age, location, etc.) and their deterioration speed. This learned relation is used to define a better prior distribution for the initial deterioration speed of each structural element. To illustrate this, Fig. 2 shows an inference example of a fully-trained SSM-BNN model providing the estimates for the deterioration state of a structural element e_p^j in the bridge $\mathcal{B}_j$. The inference process starts with transforming the visual inspection data $\tilde{\boldsymbol{y}}_{t,p}^j = [\tilde{y}_{1,p}^j \ \dots \ \tilde{y}_{\mathtt{T},p}^j]^\intercal \in [l, u]$ into an unbounded domain $\boldsymbol{y}_{t,p}^j = [y_{1,p}^j \ \dots \ y_{\mathtt{T},p}^j]^\intercal \in (-\infty, \infty)$ using the space transformation function $o(\cdot)$ detailed in Appendix C. Here, l represents the worst damage condition and u represents the perfect condition. Simultaneously, the BNN model relies on the structural attributes associated with e_p^j to provide an estimate for the initial deterioration speed $\dot{x}_{0,p}^j \sim \mathcal{N}(\dot{\mu}_z, \dot{\sigma}_z)$. After defining the element's initial state $\boldsymbol{x}_{0,p}^j$, it is passed into the KF, together with the element's transformed observations $\boldsymbol{y}_{t,p}^j$. The KF then predicts the deterioration state of the element over time $\{\boldsymbol{x}_{0,p}^j, \dots, \boldsymbol{x}_{\mathtt{T},p}^j\}$, where $\mathtt{T}$ denotes the time-horizon of the prediction. At each time step of the KF, the deterioration speed $\dot{x}_{t,p}^j$ is ensured to be negative by requiring that $\dot{\mu}_{t,p}^j + 2\dot{\sigma}_{t,p}^j \leq 0$ [6]. If this condition is not satisfied, the deterioration speed is constrained to the negative domain by truncating its PDF [6,27]. Following the completion of the KF, the RTS smoother is used to refine the KF state estimates. The smoothed state estimates and the estimated uncertainties associated with each observation are then back-transformed to the original space $\{\tilde{\boldsymbol{x}}_{0,p}^j, \dots, \tilde{\boldsymbol{x}}_{\mathtt{T},p}^j\}$ using the inverse of the transformation function $o^{-1}(\cdot)$ (see Appendix C).

Note that defining the initial state of an element $\boldsymbol{x}_{0,p}^j = [x_{0,p}^j \ \dot{x}_{0,p}^j \ \ddot{x}_{0,p}^j]^\intercal$ is an important aspect that affects the quality of the KF predictions, since there are only few observations (or inspections) per element. Accordingly, the role of the BNN model is to enhance the estimation of the prior distribution by recursively learning a mapping between the inferred deterioration speed values and the structural

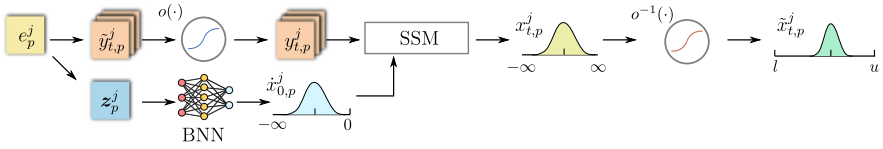


Fig. 2. Overview of the inference procedure for estimating the deterioration state of the pth element from the jth bridge, denoted by e_p^j, using the proposed SSM-BNN framework. The original visual inspections of the element $\tilde{y}_{t,p}^j$ are first transformed into an unbounded domain using the sigmoid function $o(\cdot)$, yielding the transformed observations $y_{t,p}^j$. The BNN then uses the structural attributes of the element $\boldsymbol{z}_p^j$ to define its initial deterioration rate $\dot{x}_{0,p}^j$. The initial state $\boldsymbol{x}_{0,p}^j$ and the transformed observations $y_{t,p}^j$ are then passed into SSM to predict the element's deterioration state over time $\boldsymbol{x}_{t,p}^j = [x_{t,p}^j \ \dot{x}_{t,p}^j \ \ddot{x}_{t,p}^j]^\intercal$ for $t \in \{1, 2, \ldots, \mathrm{T}\}$, where T denotes the time-horizon of the prediction. These predicted states are finally back-transformed to the original space using $o^{-1}(\cdot)$, resulting in $\tilde{\boldsymbol{x}}_{t,p}^j = [\tilde{x}_{t,p}^j \ \tilde{\dot{x}}_{t,p}^j \ \tilde{\ddot{x}}_{t,p}^j]^\intercal$.

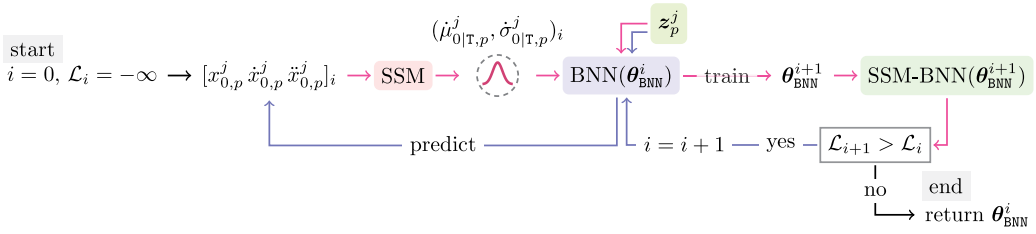


Fig. 3. The recursive process to learn the BNN model parameters θ_{BNN}. At $i = 0$, the initial states $[x_{0,p}^j \ \dot{x}_{0,p}^j \ \ddot{x}_{0,p}^j]_i$ are passed to the SSM to obtain the smoothed initial speeds $(\dot{\mu}_{0|\mathrm{T},p}^j, \dot{\sigma}_{0|\mathrm{T},p}^j)_i$. These are then used to train the BNN, so that it learns to predict them based on the structural attributes $\boldsymbol{z}_p^j$. The SSM-BNN model then evaluates the log-likelihood of the validation set $\mathcal{L}_{i+1}$ and compares it to the previous iteration $\mathcal{L}_i$. If there is an improvement, the BNN uses the structural attributes $\boldsymbol{z}_p^j$ to define the priors for the initial deterioration speeds $\dot{x}_{0,p}^j$, and the recursive loop is continues until no further improvements in $\mathcal{L}_i$.

attributes $\boldsymbol{z}_p^j$ of each structural element. Further details about the recursive learning procedure and initial state estimation are provided in the next section.

4.2. Recursively learning the BNN model parameters

The parameters of the BNN are learned using a recursive procedure due to the fact that the target variable (the deterioration speed) is not directly observed but rather is inferred. Fig. 3 illustrates the steps of the recursive parameter estimation procedure. Initially, at iteration $i = 0$, the state vector for each structural element is defined by $\boldsymbol{x}_{0,p}^j \sim \mathcal{N}(\boldsymbol{\mu}_{0,p}^j, \boldsymbol{\Sigma}_{0,p}^j)$, with the expected value relying mainly on the observation $y_{1,p}^j$ at time $t = 1$ such that, $\boldsymbol{\mu}_{0,p}^j = \left[y_{1,p}^j, 0, 0\right]^\intercal$ while the covariance is defined as $\boldsymbol{\Sigma}_{0,p}^j = \mathrm{diag}\left((\sigma_{0,p}^j)^2, (\dot{\sigma}_{0,p}^j)^2, (\ddot{\sigma}_0)^2\right)$. The initial state vector $\boldsymbol{x}_{0,p}^j$ of each element e_p^j is passed into the SSM framework composed of the Kalman filter and smoother. The Kalman smoother (backward component in SSM) returns the smoothed estimates of the initial deterioration speed $f(\dot{x}_{0,p}^j | y_{1:\mathrm{T},p}^j) = \mathcal{N}\left(\dot{\mu}_{0|\mathrm{T},p}^j, (\dot{\sigma}_{0|\mathrm{T},p}^j)^2\right)$. Thereafter, the BNN model is trained using $\dot{\boldsymbol{x}}_{0|\mathrm{T}}$ as a target variable and the structural attributes as covariates. Following the BNN training step, the BNN model is used to provide only the expected value for the initial speed such that, $\boldsymbol{\mu}_{0,p}^j = \left[y_{1,p}^j, \dot{\mu}_{z,p}^j, 0\right]^\intercal$, while the initial covariance matrix $\boldsymbol{\Sigma}_{0,p}^j$ remains the same. This is done to avoid having initial variances of the deterioration speed that are too small during the recursive learning procedure. The steps of obtaining the smoothed initial speed estimates $(\dot{\mu}_{0|\mathrm{T},p}^j, \dot{\sigma}_{0|\mathrm{T},p}^j)$ and updating the BNN model parameters are repeated until there is no improvement in the log-likelihood $\mathcal{L}$ of the validation set. Note that an update to the BNN model parameters implies that the training will start from the previous state and not from a random initial state. Furthermore, the training of the BNN model is done using tractable approximate Gaussian inference (TAGI) which is a sampling-free and gradient-free approach to learn the BNN model parameters [28].

4.3. Deterioration model parameters & hyper-parameters

The parameters of the SSM-BNN model can be grouped in the set $\boldsymbol{\theta}$ which includes, $\boldsymbol{\theta} = \{\theta_V, \sigma_W, \boldsymbol{\theta}_{\mathrm{BNN}}, \boldsymbol{\theta}_0\}$. The set $\boldsymbol{\theta}_V$ corresponds to the observation error parameters, where each inspector has a unique error term defined by the expected value μ_{V_i} and standard deviation σ_{V_i} [9]. The parameter σ_W represents the standard deviation of the process noise, and the parameters set $\boldsymbol{\theta}_{\mathrm{BNN}}$ corresponds to the weights and biases of the BNN model. The set $\boldsymbol{\theta}^0$ contains the parameters associated with the initial covariance matrix $\boldsymbol{\Sigma}_{0,p}^j$, which are adopted from a previous work by Hamida and Goulet [6]. The parameters in $\boldsymbol{\theta}^0$ include the variance of the initial condition σ_0^2, initial acceleration $\ddot{\sigma}_0^2$, and $\{p_1, p_2\}$ which define a linear relation between the variance of the deterioration speed and the deterioration condition as in, $\dot{\sigma}_0^2 = p_1^2\left(u - \tilde{\mu}_1\right) + p_2^2$. The intuition of the linear model is to counteract the low number of observations in the time series by incorporating an informative prior, so that the elements with a near perfect condition $(u - \tilde{\mu}_1 \approx 0)$ will have a lower uncertainty about their deterioration speed compared to worn out elements, where $\tilde{\mu}_1$ corresponds to the expected value of the condition at time $t = 1$ [6]. Furthermore, the acceleration prior is defined by an expected value $\ddot{\mu}_{0,p}^j = 0$ and a variance $\left(\ddot{\sigma}_{0,p}^j\right)^2 \in \boldsymbol{\theta}^0$ [6].

The hyper-parameters of the SSM-BNN include the space transformation parameter n, which governs the shape of the transformation function $o(\cdot)$ used to bound the hidden states and observations [6], and the γ scaling factor which affects the variance of the deterioration speed, and is only applied at the first iteration of the recursive estimation procedure described earlier. The scaling factor can be determined empirically from the range $[1, 10]$, and is multiplied by the parameter value p_1 in order to provide a broader prior for $\dot{x}_{0,p}^j$, enabling the SSM model to have higher flexibility in updating $\dot{x}_{t,p}^j$ during the initial stage of recursive estimation.

4.4. Estimation of the SSM-BNN parameters

The computational efficiency of the BNN model enables formulating a new parameters estimation scheme that offers better generalizability. Unlike the existing parameter estimation framework which only allows learning the model parameters using data from one structural category at a time (e.g., beams only), the new parameters estimation framework enables learning model parameters while taking into account information from all structural categories at once. This is especially important when estimating the inspectors parameters, where in a single structural

category (e.g., bridge deck) an inspector may have few data points compared to other structural categories (e.g., beams).

Accordingly, the proposed parameter estimation framework updates the inspectors parameters θ^V based on data from all structural categories, while the remaining model parameters are specific to each structural category. The estimation procedure is divided into three stages: (1) estimation of the inspectors' parameters $\theta_V = \{\mu_{V_{1:\mathrm{I}}}, \sigma_{V_{1:\mathrm{I}}}\}$, (2) estimation of the process noise σ_W along with the initial covariance parameters $\theta_0 = \{\sigma_0, \ddot{\sigma}_0, p_1, p_2\}$, and (3) estimation of the BNN model parameters θ_{BNN}. In each of the aforementioned stages, a *maximum log-likelihood estimate (MLE)* approach is utilized in the parameter estimation [6], with the log-likelihood function defined as,

$$\mathcal{L}(\theta) = \sum_{j=1}^{\mathrm{B}} \sum_{p=1}^{\mathrm{E}_j} \sum_{t=1}^{\mathrm{T}_p} \ln f(y^j_{t,p} | y^j_{1:t-1,p}, \theta), \tag{7}$$

where B denotes the total number of bridges in the network, E_j denotes the number of structural elements in the jth bridge, and T_p denotes the number of inspections for the pth element in the jth bridge. The full parameter estimation procedure is summarized in Algorithm 1.

Algorithm 1: A pseudocode for the parameter estimation process.

```
for n ∈ {1, 2, 3, 4, 5} do
    for C_m ∈ {beams, slabs, columns, ...} do
        optimize θ_0^(m), σ_W^(m), σ_V^(m) using NR;
    while Δ Σ_m L_(m) ≥ 0.1% do
        optimize θ_V = {μ_{V_{1:I}}, σ_{V_{1:I}}} using AGVI;
        for C_m ∈ {beams, slabs, columns, ...} do
            while ΔL_(m) ≥ 0.1% do
                optimize θ_0^(m), σ_W^(m) using NR;
                optimize θ_BNN^(m) using recursive estimation
return θ, n
```

The parameter estimation starts by assigning a value to the hyperparameter n which is an integer defined in the range $n \in \{1, 2, 3, 4, 5\}$ [6]. For each structural category $C_m \in \{beams,\ slabs,\ columns,\ ...\}$, a preliminary parameter estimation step is performed to learn the parameters $\sigma_W^{(m)}, \theta_0^{(m)}$ and $\sigma_V^{(m)}$ which represents to standard deviation of the observation error. Initially, all inspectors are assumed to have the same observation error defined by $V_i \sim \mathcal{N}(0, (\sigma_V^c)^2)$ [6]. Estimating the aforementioned parameters is done using the Newton–Raphson (NR) gradient optimization algorithm while relying on Eq. (7).

Following this preliminary step, the observation error is further refined by quantifying the observation error associated with each inspector. The estimation of θ_V is performed using the approximate Gaussian variance inference (AGVI), which is adopted from the work of Blanche et al. [9]. The use of AGVI in this framework remains fundamentally the same, with the sole distinction being the inclusion of inspector's inspection data from all structural categories, as opposed to a singular structural category. This modification allows for a unified set of inspectors' uncertainty parameters across all structural categories; which is different from previous applications where each structural category had a distinct set of inspector uncertainty parameters [9,29]. Further details about learning the inspectors uncertainties and the AGVI approach are provided in Appendix D.

Following the estimation of θ_V, the BNN model parameters θ_{BNN} are estimated using the recursive estimation approach described earlier. The sequential estimation of θ_V, θ_0, $\sigma_W^{(m)}$, and θ_{BNN} is repeated until the improvement in the overall validation-set log-likelihood is negligible (e.g., $\leq 0.1\%$). It should be noted that the validation set is an independent set, where the structural elements of the same structure are not simultaneously present in the training set and the test set.

5. Case studies

The case studies rely on real data from the network of bridges in Quebec, Canada, as well as synthetic data generated for verification purposes.

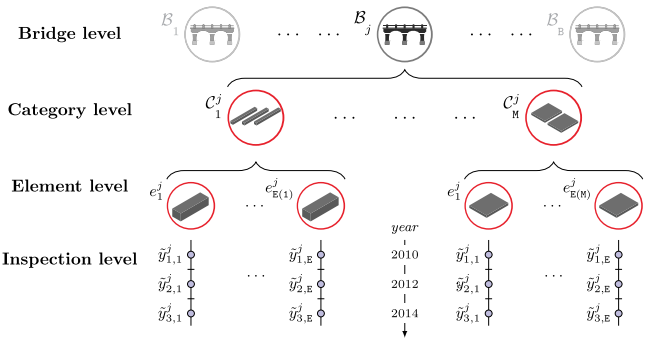


Fig. 4. Graphical illustration of the components making up the bridge database, with each bridge $\mathcal{B}_j$ encompassing multiple structural categories C^j_m and each category containing multiple structural elements. The visual inspections are performed on an element level, whereby an element e^j_p is assigned a condition rating of $\tilde{y}^j_{t,p}$ at the time step t.

Table 1
Summary of the structural attributes associated with each structural element.

Covariates	Value ranges	Unit
$z^j_{p,1}$: material	[0, 1]	–
$z^j_{p,2}$: age	[0, 165]	years
$z^j_{p,3}$: latitude	[44.99, 58.67]	–
$z^j_{p,4}$: average health condition	[28, 100]	–
$z^j_{p,5}$: longitude	[−79.51, −57.25]	–
$z^j_{p,6}$: total length	[3.674, 1801.4]	meters
$z^j_{p,7}$: slab length	[3.674, 1801.4]	meters
$z^j_{p,8}$: total width	[3.35, 120]	meters
$z^j_{p,9}$: surface area	[17, 52420]	square meters
$z^j_{p,10}$: number of lanes	[0, 13]	lanes
$z^j_{p,11}$: percentage of trucks	[0, 100]	–
$z^j_{p,12}$: annual average daily traffic	[0, 178000]	vehicle per day

5.1. Data description

5.1.1. Real data

In this paper, infrastructure deterioration is modeled based on visual inspections and structural attributes from a network of approximately 10000 bridges located in the province of Quebec, Canada. The hierarchy of the data is illustrated in Fig. 4, where each bridge $\mathcal{B}_j$ is made up of different structural categories $\{C^j_1, \ldots, C^j_m, \ldots, C^j_{\mathrm{M}}\}$, and each structural category is composed of multiple structural elements, $C^j_m = \{e^j_1, \ldots, e^j_p\}$. The visual inspection data denoted by $\tilde{y}^j_{t,p}$ correspond to observations of the elements's health condition over time t. In this context, $\tilde{y}$ is defined on a continuous domain, where $\tilde{y} = 100$ represents a perfect condition and $\tilde{y} = 25$ signifies the poorest condition. The inspection frequency differs from one bridge to another, with ranges from once a year to once every five years [30]. In total, the majority of the bridges have four or five inspections performed in the period from 2007 to 2023.

The structural attributes associated with each structural element e^j_p are denoted by z^j_p and correspond to the material of the structural element, age, latitude, longitude, total length of the bridge, slab length, total width of the bridge, surface area, number of lanes, percentage of trucks, annual average of daily traffic (AADT) and average health condition. A summary for the structural attributes considered in this study is provided in Table 1.

5.1.2. Synthetic data

The synthetic data utilized in this study has comparable quantitative and qualitative characteristics to the real visual inspection data. The quantitative similarities include similarities in the number of synthetic

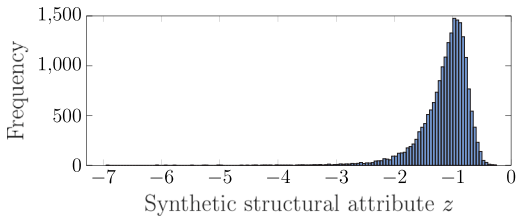


Fig. 5. Histogram of the synthetic structural attribute generated using $z^j = \ln(|\dot{x}_0^j|) + w_0$, $w_0 : W_0 \sim \mathcal{N}(0, 0.1^2)$ adopted from the work of Hamida and Goulet [24].

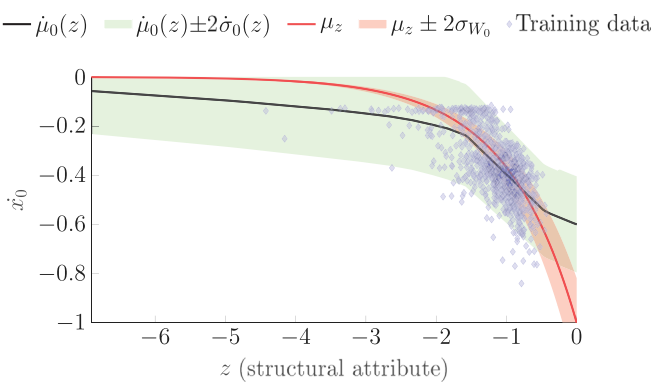


Fig. 6. The latent relation between the synthetic structural attribute z and the deterioration speed $\dot{x}_0$ learned by the BNN. The black line represents the expected values predicted by the BNN with the shaded green area representing uncertainty. The true relation is depicted by the red line with the shaded red area representing its variability. Having this variability makes the synthetic attributes resemble reality, where structures with different attributes can deteriorate at the same speed.

structural elements, the number of inspections per structural element, and the total number of unique observation errors (i.e., number of inspectors). The qualitative similarities on the other hand equates to similarity in the deterioration curve over time and the average life span of the structural element [6].

In this paper, a total of $\mathtt{E} = 20000$ synthetic beam elements are considered, with each element having 4 to 5 inspections over a time span of 10 years. The elements deterioration curves are designed to have an average service life of 60 years. The total number of synthetic inspectors is $\mathtt{I} = 300$, with each inspector's error defined by $v_i : V_i \sim \mathcal{N}(\mu_{V_i}, \sigma^2_{V_i})$. The true deterioration curves for each synthetic element are generated using the transition model defined in Eq. (1) with the standard deviation of the process noise set to $\sigma_W = 5 \times 10^{-3}$. While the synthetic inspection data is generated using the observation model defined in Eq. (3) by sampling synthetic observations from the true synthetic deterioration states. The parameters associated with the observation errors of inspectors are sampled from uniform distributions, following $\mu_{V_i} \sim \mathcal{U}(-4, 4)$ and $\sigma_{V_i} \sim \mathcal{U}(1, 6)$. To ensure that the deterioration curves exhibit the same qualitative characteristics of the real deterioration, several criteria are enforced on the synthetic elements' states, which are adopted from the work of Hamida and Goulet [6]. Alongside the synthetic visual inspection data, a synthetic structural attribute z^j is generated using: $z^j = \ln(|\dot{x}_0^j|) + w_0$, where w_0 is an error term described by $w_0 : W_0 \sim \mathcal{N}(0, 0.1^2)$, [24]. This relation results in unevenly distributed synthetic attribute z^j with a long-tail distribution (see Fig. 5), allowing to effectively verify the robustness of the proposed framework.

5.2. Verification of the SSM-BNN model using synthetic data

The SSM-BNN framework is verified on synthetic data using a neural network architecture and configuration defined in Appendix A. In this example, the BNN model is trained with a single input variable corresponding to the synthetic structural attribute z^j, and a single output variable which is the deterioration speed. The training data is split into training and validation sets using an 85/15 split to avoid overfitting, and is standardized to have a zero mean and unit variance.

The parameters of the SSM-BNN model are estimated using the steps described in the pseudocode in Algorithm 1. While all the steps in the pseudocode are equally important, this section will focus mainly on the capacity of the BNN model in learning the relationship between the synthetic structural attribute z^j and the deterioration speed. Fig. 6 illustrates the latent relation between the synthetic structural attribute z^j and the initial deterioration speed $\dot{x}_0$ as learned by the BNN model, along with the training data and the ground truth.

From Fig. 6, the training data represented by the blue diamond-shapes corresponds to the smoothed estimates of the initial deterioration speed $\dot{\boldsymbol{x}}_{0|\mathtt{T}}$ for each synthetic structural elements. On the other hand, the red curve represents the true relation between $\dot{\boldsymbol{x}}_{0|\mathtt{T}}$ and $\boldsymbol{z}^j$. The BNN model inference for the aforementioned relation is depicted by the black line with the green confidence interval. The BNN model inference is achieved by relying on the recursive estimation procedure described in Section 4.2. From Fig. 6, the true speed lies within two standard deviations of the mean predicted by the BNN for nearly the full range of inputs, in spite of the input $\boldsymbol{z}^j$ having a range of values $\boldsymbol{z}^j \in [-7, -2]$ with a lower density of training data.

A time-series example that demonstrates the performance of the trained SSM-BNN model is shown in Fig. 7. From this figure, the true state of the deterioration speed represented by the black dashed-line is within the confidence interval of the SSM-BNN model, despite the high variability in the inspections.

The performance of the SSM-BNN model is compared against the existing SSM-KR model, which is configured based on the work of Hamida and Goulet [24]. The performance comparison focuses on the predictive capacity of each model in estimating the initial deterioration speed as well as the total time required for estimating the model parameters. The training time of the SSM-BNN model is approximately 0.5 h that is required to learn the full set of parameters, while the SSM-KR needed approximately 1 hour. Fig. 8 shows a scatter plot for the two models predictions versus the true initial speed values, generated based on a random sample of 500 synthetic structural elements.

From Fig. 8 it is shown that the estimates of the SSM-BNN model have a better alignment with the true deterioration speed values, especially for lower deterioration speeds (i.e., $\dot{x}_0 < -0.3$). This is demonstrated by the equal spread of the SSM-BNN predictions around the diagonal line.

5.3. Validation of the SSM-BNN using real data

The proposed SSM-BNN model is initially trained using the visual inspection data and the structural attributes $z^j_{p,1:12}$ of beam structural elements from $\mathtt{B} = 5998$ bridges. The visual inspections in the aforementioned dataset are performed by $\mathtt{I} = 311$ inspectors. The beams's dataset encompass a training set with $\mathtt{E}_{\mathtt{tr}} = 48517$ elements, a validation set with $\mathtt{E}_{\mathtt{val}} = 2178$ elements, and a test set with $\mathtt{E}_{\mathtt{ts}} = 1089$. The architecture and configuration of the BNN model are described in Appendix A.

Similar to the synthetic case, the input covariates and the response variable are standardized to have zero mean and unit variance. The output of the BNN model is a single variable representing the deterioration speed $\dot{x}^j_{0,p}$ at time $t = 0$, while the total number of the input covariates is $\mathtt{Z} = 18$. The input covariates correspond to a one-hot encoded material covariate in addition to 11 structural attributes $z^j_{p,2:12}$ defined in Table 1. The material in the case of beam elements includes: weathering steel, regular steel, aluminum, wood, high-performance concrete, prestressed concrete, and regular concrete. An example that demonstrates the SSM-BNN model performance on a beam element

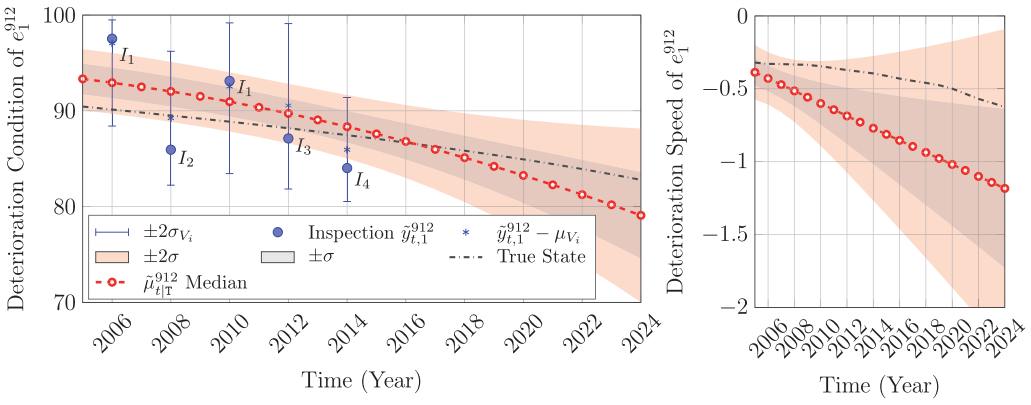


Fig. 7. Estimates of deterioration state for condition (left) and deterioration speed (right) based on synthetic inspection data $\tilde{\mathbf{y}}_{t,1}^{912} \in [25, 100]$ represented by the blue points. Error bars represent the synthetic inspectors' uncertainty estimates, while the black dashed-line correspond to the true state of deterioration.

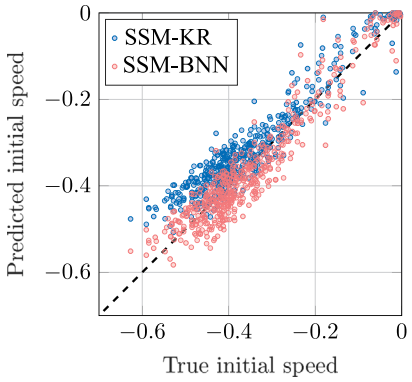


Fig. 8. Scatter plot and histogram comparing the true initial deterioration speeds $\dot{x}_0$ of the synthetic elements with those predicted by SSM-BNN and SSM-KR.

Table 2
A comparison between SSM-KR and SSM-BNN based on the log-likelihood and the training time. The log-likelihood is estimated using hidden inspection points, each taken from an independent test set of approximately 1000 beam elements.

Model	Log-likelihood	Total training time (hrs)
SSM-KR	−14180	189
SSM-BNN	**-13364**	**3**

is shown in Fig. 9, where the model estimates are updated using 4 inspection points represented by the blue circles. The inspection point represented by the black square is a hidden inspection data, which is only used for validating the model predictive capacity and is not used in updating or estimating the model parameters.

From Fig. 9, the hidden inspection point is within the confidence interval of the SSM-BNN model forecast. Note that matching the observation is not necessarily equivalent to matching the true state, as the hidden inspection point has a relatively large uncertainty as shown in Fig. 9.

The analyses from the previous example are expanded to include multiple beam elements by estimating the sum of the log-likelihood for a subset of hidden inspection data points. Accordingly, a subset of approximately 1000 beam elements is considered in the analyses, where the log-likelihood is estimated for the last hidden inspection point, and the total sum of the log-likelihoods is reported in Table 2 for the SSM-BNN and the SSM-KR. The SSM-KR in this instance is trained using 4 attributes (material, age, location represented by the latitude and the health condition at time $t = 1$), and is configured based on the work of Hamida and Goulet [24].

From Table 2, the SSM-BNN model achieves 6% improvement in the log-likelihood over the SSM-KR, while being nearly two orders of magnitude faster in training time. Note that the training times for the real and synthetic data are measured while using a system equipped with an Intel Xeon 6248R CPU, 256 GB memory, and a NVIDIA Quadro RTX 5000 GPU.

5.4. Large-scale application of the SSM-BNN model

As mentioned in the methodology section, the SSM-BNN model benefits from a new parameter estimation procedure that allows having a unified set of inspector's parameters $\boldsymbol{\theta}_V$ across multiple structural categories. In this experiment, the scope of the analyses is limited to five structural categories: C_1 : exterior walls, C_2 : front walls, C_3 : slabs, C_4 : beams, and C_5 : pavement. In total, there are $\mathtt{I} = 325$ inspectors responsible for performing inspections across all bridges, with each structural category C_m having approximately $\mathtt{I}_m \approx 300$ inspectors. Accordingly, it is very likely for each inspector I_i to perform inspections on different structural categories. For example, inspector $I_{i=3}$ can be responsible for performing the inspections on beams, slabs and front walls in different years and on different bridges.

The existing parameter estimation procedure assumes that each structural category has a distinct set of parameters defined as in, $\boldsymbol{\theta}_{\text{exist}} = \{\boldsymbol{\theta}_V^{(1:5)}, \sigma_W^{(1:5)}, \boldsymbol{\theta}_{\text{BNN}}^{(1:5)}, \boldsymbol{\theta}_0^{(1:5)}\}$, where the superscript $^{(n:m)}$ is a reference to the structural category index from C_1 to C_5 [29]. Inherently, this approach assumes a unique set of inspectors parameters $\boldsymbol{\theta}_V^m$ associated with each structural category C_m, which ignores the fact that the same inspector could be responsible for inspections on other structural categories. To overcome this limitation, the new parameter estimation procedure learns the parameters of each inspector I_i based on data from all structural categories, which results in a unified set of inspectors' parameters $\boldsymbol{\theta}_V$, where $\boldsymbol{\theta}_V = \{\mu_{V_{1:\mathtt{I}}}, \sigma_{V_{1:\mathtt{I}}}\}$. Accordingly, the model parameters using the new approach are defined as in, $\boldsymbol{\theta} = \{\boldsymbol{\theta}_V, \sigma_W^{(1:5)}, \boldsymbol{\theta}_{\text{BNN}}^{(1:5)}, \boldsymbol{\theta}_0^{(1:5)}\}$. In order to demonstrate the effectiveness of the new parameter estimation procedure, the performance of SSM-BNN($\boldsymbol{\theta}_{\text{exist}}$) and SSM-BNN($\boldsymbol{\theta}$) are evaluated using the log-likelihood. Table 3 shows the log-likelihoods estimates for the validation and test sets.

From Table 3, the model SSM-BNN($\boldsymbol{\theta}$) with the parameters estimated using the new approach performs better on three out of the five structural categories on the validation set and four out of the five structural categories on the test set. These results indicate that the inspectors' parameters estimated with the new approach generalize better on the independent test sets. Furthermore, the results indicates that training on each structural category independently may induce overfitting (e.g., exterior walls and pavement have better validation log-likelihood and worse test log-likelihood). Training the SSM-BNN model using data from all the structural categories significantly increases the number of observations per inspector, which contributes to bringing their estimated parameters closer to the true values. This is supported by the model trained using the unified set $\boldsymbol{\theta}_V$ achieving better log-likelihoods on most of the validation and test sets (Table 3).

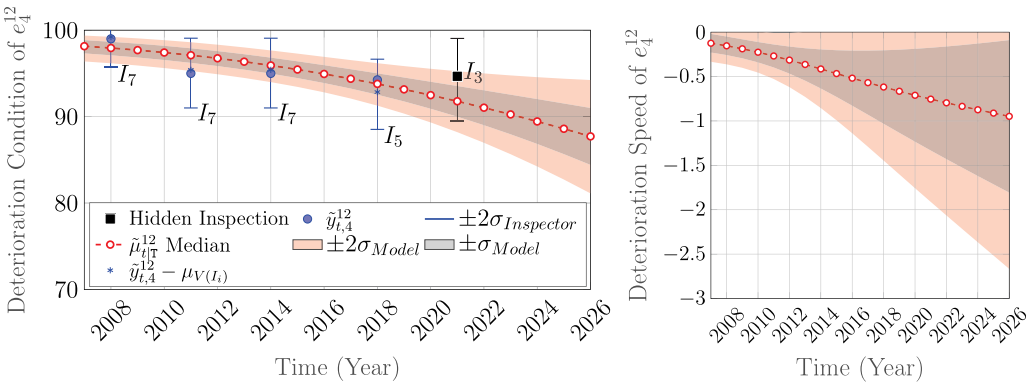


Fig. 9. Estimates of deterioration state for condition (left) and deterioration speed (right) based on inspection data $\tilde{y}_{t,4}^{12} \in [25, 100]$ represented by the blue points. Error bars represent the inspectors' uncertainty estimates, while the black square correspond to a hidden inspection for testing.

Table 3
Comparison of the SSM-BNN(θ) versus the SSM-BNN(θ_{exist}) using five structural categories. The log-likelihood of the SSM-BNN(θ_{exist}) is denoted by $\mathcal{L}_{\text{exist}}$ while the log-likelihood of the joint approach is denoted by $\mathcal{L}$. Bold numbers indicate better performance.

Category	Validation set		Test set	
	$\mathcal{L}_{\text{exist}}$	$\mathcal{L}$	$\mathcal{L}_{\text{exist}}$	$\mathcal{L}$
Exterior walls	**−1.16E+04**	**−1.20E+04**	−5.47E+03	**−5.44E+03**
Front walls	−5.79E+03	**−5.75E+03**	−2.94E+03	**−2.92E+03**
Slabs	−8.18E+03	**−8.13E+03**	−3.02E+03	**−2.93E+03**
Beams	−2.12E+04	**−2.10E+04**	**−1.23E+04**	−1.25E+04
Pavement	**−6.64E+03**	−7.02E+03	−4.69E+03	**−3.32E+03**

6. Conclusion

This paper proposed a new probabilistic framework for modeling the deterioration of large transportation infrastructure based on visual inspections and structural attributes. The proposed framework relies on a state-space model (SSM) coupled with a Bayesian neural network (BNN) that enables incorporating structural attributes in the deterioration analyses. The SSM-BNN model is trained using a new estimation approach that significantly reduces the number of model parameters. The performance of the SSM-BNN model is verified using synthetic data and validated using real inspection from the network of bridges in Quebec, Canada. The results of the analyses from synthetic data highlights the capacity of the SSM-BNN model in quantifying the relationship between the inferred deterioration speed and the structural attributes. In addition, the SSM-BNN model predictions have a better alignment with the true synthetic speed in comparison to the existing SSM-KR framework. As for the real data, the comparison with the existing SSM-KR shows that the proposed SSM-BNN model achieves approximately 6% improvement in the log-likelihood, while requiring significantly lower training time (3 h compared to 189 h). Those advantages have facilitated the implementation of a new parameter estimation procedure that enabled reducing the total number of model parameters while improving the overall generalizability of the model. This is demonstrated through comparisons among the models' log-likelihood estimates on independent validation and test sets. Despite the highlighted advantages in the SSM-BNN model, the use of BNN remains limited to quantifying the initial deterioration speed only. Future work can address this limitation by using frameworks such as LSTM [31], to provide state estimates for timestamps beyond the initial deterioration speed.

CRediT authorship contribution statement

Said Ali Kamal Fakhri: Writing – original draft, Visualization, Validation, Methodology, Investigation, Formal analysis. **Zachary Hamida:** Writing – review & editing, Supervision, Software, Methodology, Data curation, Conceptualization. **James-A. Goulet:** Writing – review & editing, Supervision, Resources, Project administration, Methodology, Funding acquisition, Conceptualization.

Funding

This project is funded by the Ministry of Transportation Quebec (MTQ). Said Ali Kamal Fakhri was supported by a scholarship from the Institute for Data Valorization (IVADO).

Declaration of competing interest

The authors declare that they have no known competing financial interests or personal relationships that could have appeared to influence the work reported in this paper.

Acknowledgment

The authors would like to acknowledge the support of Simon Pedneault for facilitating the access to information related to this project.

Appendix A. BNN configuration and training

The architecture employed for the BNN model consists of one hidden layer with 128 units, with a ReLU activation function. The weights and biases of the BNN are initialized using He's method [32], and the batch size during the training is 16 instances. The approach used in learning the BNN model parameters is tractable approximate Gaussian inference (TAGI) [28,33]. The use of TAGI in the context of a fully-connected feedforward neural network (FNN) consists of inputs $\boldsymbol{s} \in \mathbb{R}^{\mathrm{S}}$ and outputs $\boldsymbol{r} \in \mathbb{R}^{\mathrm{R}}$ connected by $\mathtt{L}$ hidden layers, graphically depicted in Fig. A.10.

These connections are established through matrix–vector multiplication and addition with the network parameters $\boldsymbol{\theta}_{\text{NN}} = \{\mathbf{W}, \boldsymbol{b}\}$, followed by a non-linear activation function $\varphi(\cdot)$. Specifically, the hidden units $\boldsymbol{h}^{(j)} \in \mathbb{R}^{|j|}$ in layer j are used to obtain the hidden units in the next layer $\boldsymbol{h}^{(j+1)} \in \mathbb{R}^{|j+1|}$ following,

$$\boldsymbol{h}^{(j+1)} = \mathbf{W}^{(j)} \left(\varphi(\boldsymbol{h}^{(j)})\right) + \boldsymbol{b}^{(j)}, \quad j = 0, 1, \ldots, \mathtt{L}, \tag{A.1}$$

where $\mathbf{W}^{(j)} \in \mathbb{R}^{|j+1|\times|j|}$ and $\boldsymbol{b}^{(j)} \in \mathbb{R}^{|j+1|}$ are the weights and biases in layer j with $|j|$ and $|j+1|$ indicating the number of units in layers j and $j+1$, respectively. Note that the activation units in layer $j = 0$ simply correspond to the inputs to the network $\boldsymbol{s} \equiv \varphi(\boldsymbol{h}^{(0)})$.

TAGI uses Eq. (A.1) to analytically propagate uncertainty forward by treating the network parameters as independent Gaussian random variables, so that $\boldsymbol{\theta}_{\text{NN}} \sim \mathcal{N}\left(\boldsymbol{\mu}_{\theta}, \mathbf{I} \cdot \boldsymbol{\sigma}_{\theta}^{2}\right)$, as well as making several other assumptions and approximations which are detailed in [28]. The

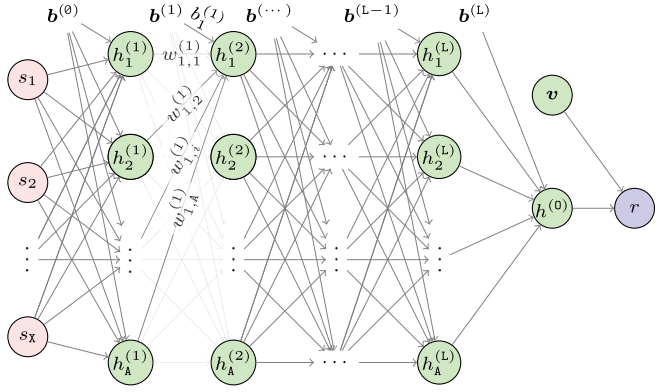


Fig. A.10. Graphical representation of a feedforward neural network consisting of L hidden layers with A hidden units in each one. The network maps the relation between the inputs $\boldsymbol{s} = [s_1 \cdots s_S]^\intercal$ and the unit at the output layer $h^{(0)}$. To simplify visualization, the output is shown here as one-dimensional. The observation r is connected to the output layer unit $h^{(0)}$ and the error term v through the observation model defined in Eq. (A.2). The parameters connecting layer j with layer $j+1$ consist of a vector of biases $\boldsymbol{b}^{(j)}$ and a matrix of weights $\mathbf{W}^{(j)}$, such that $w_{m,i}^{(j)} \in \mathbf{W}^{(j)}$ represents the weight connecting the ith unit in layer j to the mth unit in layer $j+1$.

relation between the network's outputs $\boldsymbol{h}^{(0)}$ and the observed system responses $\boldsymbol{r}$ is described by the following observation model,

$$\boldsymbol{r} = \boldsymbol{h}^{(0)} + \boldsymbol{v},\ \boldsymbol{v} : \boldsymbol{V} \sim \mathcal{N}\left(\mathbf{0}, \mathbf{I} \cdot \sigma_V^2\right), \tag{A.2}$$

where $\boldsymbol{v}$ represents independent zero-mean Gaussian errors. TAGI performs closed-form inference using the equations for the Gaussian conditional and Rauch–Tung–Striebel (RTS) smoother [26], which are detailed in Appendix B. Given that TAGI initializes the network parameters with a weakly informed prior, the inference is performed over multiple successive passes over the training set. To prevent overfitting, this iterative learning process is stopped once the likelihood on the validation set stops improving. The use of TAGI in this paper enables the analytical inference of the heteroscedastic observation error variance, the neural network's parameters and hidden units [33].

Appendix B. Kalman filter and Rauch–Tung–Striebel smoother

Kalman filter (KF) [25] estimates the deterioration state at each time step t using the prediction and update steps. The prediction step estimates the state $\boldsymbol{x}_t$ from $\boldsymbol{x}_{t-1}$ using the transition model from Eq. (1), such that,

$$\begin{aligned} \boldsymbol{\mu}_{t|t-1} &= \mathbf{A}\boldsymbol{\mu}_{t-1|t-1}, \\ \boldsymbol{\Sigma}_{t|t-1} &= \mathbf{A}\boldsymbol{\Sigma}_{t-1|t-1}\mathbf{A}^\intercal + \mathbf{Q}. \end{aligned} \tag{B.1}$$

Here, $\boldsymbol{\mu}_{t|t-1} \equiv \mathbb{E}[\boldsymbol{X}_t|y_{1:t-1}]$ and $\boldsymbol{\Sigma}_{t|t-1} \equiv \mathrm{cov}[\boldsymbol{X}_t|y_{1:t-1}]$ are the expected value and covariance for the state at time t, given all the observations up to time $t-1$, which are denoted by $y_{1:t-1} \equiv \{y_1, y_2, \ldots, y_{t-1}\}$. In the absence of an observation at time t, the prediction step is repeated; otherwise, if an observation is available, the update step is applied. The update step finds the posterior knowledge of $\boldsymbol{x}_t$ conditioned on all the observations $y_{1:t}$ using the Gaussian conditional equations.

Once the state estimates are obtained by the KF, they are then refined using the Rauch–Tung–Striebel (RTS) smoother [26], which is given by the following equations:

$$\begin{aligned} f\left(\boldsymbol{x}_t \mid y_{1:\mathrm{T}}\right) &= \mathcal{N}\left(\boldsymbol{x}_t; \boldsymbol{\mu}_{t|\mathrm{T}}, \boldsymbol{\Sigma}_{t|\mathrm{T}}\right), \\ \boldsymbol{\mu}_{t|\mathrm{T}} &= \boldsymbol{\mu}_{t|t} + \mathbf{J}_t\left(\boldsymbol{\mu}_{t+1|\mathrm{T}} - \boldsymbol{\mu}_{t+1|t}\right), \\ \boldsymbol{\Sigma}_{t|\mathrm{T}} &= \boldsymbol{\Sigma}_{t|t} + \mathbf{J}_t\left(\boldsymbol{\Sigma}_{t+1|\mathrm{T}} - \boldsymbol{\Sigma}_{t+1|\mathrm{T}}\right)\mathbf{J}_t^\intercal, \\ \mathbf{J}_t &= \boldsymbol{\Sigma}_{t|t}\mathbf{A}^\intercal\boldsymbol{\Sigma}_{t+1|t}^{-1}, \end{aligned} \tag{B.2}$$

where $\boldsymbol{\mu}_{t|\mathrm{T}}$ and $\boldsymbol{\Sigma}_{t|\mathrm{T}}$ are the posterior mean and covariance of the smoothed state estimates at time t, given all the observations up to time T, which denotes the time step of the last observation.

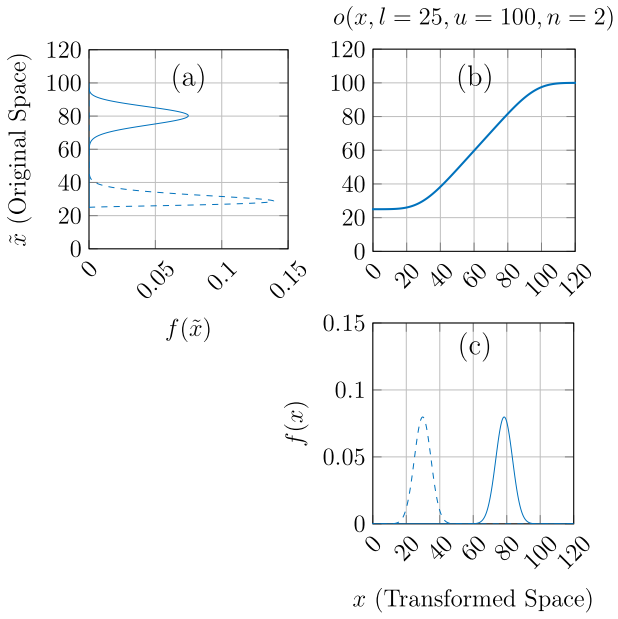


Fig. C.11. Example of space transformation on two probability density functions (PDF), one represented by a continuous line and the other by a dashed line. The example demonstrates the effect of the non-linear transformation function in Fig. C.11(b) on the shape of each PDF.
Source: The figure is reproduced from the work of Hamida and Goulet [6].

Appendix C. Space transformation

The original observations $\tilde{x} \in [l, u]$ are transformed into an unbounded domain $x \in (-\infty, \infty)$ using the following function,

$$o(\tilde{x}) = \begin{cases} \left[\frac{1}{\Gamma(\alpha)}\int_0^{\tilde{x}} t^{\alpha-1}e^{-t}dt\right]^\alpha, & \frac{u+l}{2} < \tilde{x} \le u, \\ \tilde{x}, & \tilde{x} = \frac{u+l}{2}, \\ -\left[\frac{1}{\Gamma(\alpha)}\int_0^{\tilde{x}} t^{\alpha-1}e^{-t}dt\right]^\alpha, & l \le \tilde{x} < \frac{u+l}{2}, \end{cases} \tag{C.1}$$

$$o^{-1}(x) = \begin{cases} \frac{1}{\Gamma(\alpha)}\int_0^{x^{\frac{1}{\alpha}}} t^{\alpha-1}e^{-t}dt, & \frac{u+l}{2} < x, \\ x, & x = \frac{u+l}{2}, \\ -\frac{1}{\Gamma(\alpha)}\int_0^{x^{\frac{1}{\alpha}}} t^{\alpha-1}e^{-t}dt, & x < \frac{u+l}{2}. \end{cases}$$

Here, $\Gamma(\cdot)$ is the gamma function and α is the shape parameter of the gamma distribution. The shape parameter is defined as $\alpha \equiv 2^{-n}$, where n is a positive integer that controls the curvature of the transformation function near the bounds l and u. After completing the inference in SSM, the predictions of the deterioration model $x \in (-\infty, \infty)$ are back-transformed into the original space $\tilde{x} \in [l, u]$ using the function $o^{-1}(x)$ in Eq. (C.1).

An example that demonstrate the transformation of a probability density function (PDF) from the transformed space to the original space is shown in Fig. C.11. In this figure the dashed-line PDF is elongated in the original space due to being near the transformation function bounds. On the other hand, the continuous line PDF maintains the same shape in both spaces due being centered in the linear segment of the transformation function. Further details about the space transformation function are available in the work of Hamida and Goulet [6].

Appendix D. Learning the uncertainty of each inspector

Each inspector I_i has a unique observation error described by $v_i : V_i \sim \mathcal{N}(\mu_{V_i}, \sigma^2_{V_i})$. Estimating μ_{V_i} and $\sigma^2_{V_i}$ is done by augmenting the state vector with two additional hidden states defined by,

$$\begin{aligned} v_{b(i)} &: V_{b(i)} \sim \mathcal{N}\left(v_{b(i)}; \mu_{b(i)}, \sigma^2_{b(i)}\right), \\ v_{s(i)} &: V_{s(i)} \sim \mathcal{N}\left(v_{s(i)}; 0, \sigma^2_{s(i)}\right), \end{aligned} \tag{D.1}$$

where the term $v_b(I_i)$ is a hidden state corresponding to μ_{V_i}, and the term $v_s(I_i)$ corresponds to $\sigma^2_{V_i}$ [9]. Quantifying these additional hidden states happens concurrently with the inference of the deterioration states in the SSM framework. Specifically, $v_{b(i)}$ and $v_{s(i)}$ are updated whenever the inspection $\tilde{y}^j_{t,p}$ is performed by the inspector I_i. The updates for $v_{b(i)}$ and $v_{s(i)}$ are performed by using the approximate Gaussian variance inference (AGVI) approach for estimating the variance hidden state $v_{s(i)}$, and a recursive framework for estimating the hidden state $v_{b(i)}$ associated with the expected value μ_{V_i}. Further details about the two approaches are provided in the work of Blanche et al. [9].

Data availability

The data that has been used is confidential.

References

[1] C. Boller, P. Starke, G. Dobmann, C.-M. Kuo, C.-H. Kuo, Approaching the assessment of ageing bridge infrastructure, Smart Struct. Syst. 15 (3) (2015) 593–608.

[2] Z. Hamida, J.-A. Goulet, Quantifying the relative change in maintenance costs due to delayed maintenance actions in transportation infrastructure, J. Perform. Constr. Facil. 38 (5) (2024) 04024035.

[3] D. Agdas, J.A. Rice, J.R. Martinez, I.R. Lasa, Comparison of visual inspection and structural-health monitoring as bridge condition assessment methods, J. Perform. Constr. Facil. 30 (3) (2015) 04015049.

[4] C. Koch, K. Georgieva, V. Kasireddy, B. Akinci, P. Fieguth, A review on computer vision based defect detection and condition assessment of concrete and asphalt civil infrastructure, Adv. Eng. Inform. 29 (2) (2015) 196–210.

[5] M. Artus, C. Koch, State of the art in damage information modeling for RC bridges–A literature review, Adv. Eng. Inform. 46 (2020) 101171.

[6] Z. Hamida, J.-A. Goulet, Modeling infrastructure degradation from visual inspections using network-scale state-space models, Struct. Control Health Monit. 27 (9) (2020) e2582, e2582 stc.2582.

[7] T. Liu, B. Li, X. Du, B. Jiang, X. Jin, L. Jin, Z. Zhao, Component-aware anomaly detection framework for adjustable and logical industrial visual inspection, Adv. Eng. Inform. 58 (2023) 102161.

[8] T. Li, M. Alipour, D.K. Harris, Context-aware sequence labeling for condition information extraction from historical bridge inspection reports, Adv. Eng. Inform. 49 (2021) 101333.

[9] B. Laurent, B. Deka, Z. Hamida, J.-A. Goulet, Analytical inference for inspectors' uncertainty using network-scale visual inspections, J. Comput. Civ. Eng. 37 (5) (2023) 04023022.

[10] X. Lei, Y. Xia, L. Deng, L. Sun, A deep reinforcement learning framework for life-cycle maintenance planning of regional deteriorating bridges using inspection data, Struct. Multidiscip. Optim. 65 (2022).

[11] Z. Hamida, J.-A. Goulet, Hierarchical reinforcement learning for transportation infrastructure maintenance planning, Reliab. Eng. Syst. Saf. 235 (2023) 109214.

[12] Z. Mirzaei, B.T. Adey, L. Klatter, J.S. Kong, Overview of Existing Bridge Management Systems-Report by the IABMAS Bridge Management Committee, Technical Report, International Association for Bridge Maintenance and Safety - IABMAS, 2012.

[13] A.K. Agrawal, A. Kawaguchi, Z. Chen, Deterioration rates of typical bridge elements in new york, J. Bridge Eng. 15 (4) (2010) 419–429.

[14] F. Wang, C.-C.B. Lee, N.G. Gharaibeh, Network-level bridge deterioration prediction models that consider the effect of maintenance and rehabilitation, J. Infrastruct. Syst. 28 (1) (2022) 05021009.

[15] I. Zambon, A. Vidovic, A. Strauss, J. Matos, J. Amado, Comparison of stochastic prediction models based on visual inspections of bridge decks, J. Civil Eng. Manag. 23 (5) (2017) 553–561.

[16] Z. Hamida, J.-A. Goulet, Quantifying the effects of interventions based on visual inspections from a network of bridges, Struct. Infrastruct. Eng. 18 (8) (2022) 1222–1233.

[17] M.R. Dann, M. Birkland, Structural deterioration modeling using variational inference, J. Comput. Civ. Eng. 33 (1) (2019) 04018057.

[18] Y.-H. Huang, Artificial neural network model of bridge deterioration, J. Perform. Constr. Facil. 24 (6) (2010) 597–602.

[19] M. Santamaria Ariza, I. Zambon, H. S. Sousa, J.A. Campos e Matos, A. Strauss, Comparison of forecasting models to predict concrete bridge decks performance, Struct. Concr. 21 (4) (2020) 1240–1253.

[20] J. Sobanjo, A neural network approach to modeling bridge deterioration, Comput. Civil Eng. (1997) 623–626.

[21] P. Rattanasuwan, Estimating NBI Ratings Using a Neural Network (Master's thesis), University of Wisconsin-Madison, Wisconsin, USA, 1998.

[22] I. Zambon, A. Vidović, A. Strauss, J. Matos, Condition prediction of existing concrete bridges as a combination of visual inspection and analytical models of deterioration, Appl. Sci. 9 (1) (2019).

[23] E.A. Dizaj, J.E. Padgett, M.M. Kashani, A Markov chain-based model for structural vulnerability assessmentof corrosion-damaged reinforced concrete bridges, Phil. Trans. R. Soc. A 379 (2203) (2021) 20200290.

[24] Z. Hamida, J.-A. Goulet, Network-scale deterioration modelling based on visual inspections and structural attributes, Struct. Saf. (2020).

[25] R.E. Kalman, A new approach to linear filtering and prediction problems, J. Basic Eng. 82 (1) (1960) 35–45.

[26] H.E. Rauch, C. Striebel, F. Tung, Maximum likelihood estimates of linear dynamic systems, AIAA J. 3 (8) (1965) 1445–1450.

[27] D. Simon, D.L. Simon, Constrained Kalman filtering via density function truncation for turbofan engine health estimation, Int. J. Syst. Sci. 41 (2) (2010) 159–171.

[28] J.-A. Goulet, L. Nguyen, S. Amiri, Tractable approximate Gaussian inference for Bayesian neural networks, J. Mach. Learn. Res. 22 (251) (2021) 1–23.

[29] Z. Hamida, J.-A. Goulet, A stochastic model for estimating the network-scale deterioration and effect of interventions on bridges, Struct. Control Health Monit. 29 (4) (2022) e2916.

[30] MTQ, Ministère des transports, de la mobilité durable et de l'électrification des transports, 2014.

[31] V.-D. Vuong, L.-H. Nguyen, J.-A. Goulet, Coupling LSTM neural networks and state-space models through analytically tractable inference, Int. J. Forecast. (2024).

[32] K. He, X. Zhang, S. Ren, J. Sun, Delving deep into rectifiers: Surpassing human-level performance on ImageNet classification, in: 2015 IEEE International Conference on Computer Vision, ICCV, 2015, pp. 1026–1034.

[33] B. Deka, L.H. Nguyen, J.-A. Goulet, Analytically tractable heteroscedastic uncertainty quantification in Bayesian neural networks for regression tasks, Neurocomputing 572 (2024) 127183.